



Data-Driven Overlapping-Track Profile Modeling in Cold Spray Additive Manufacturing

Daiki Ikeuchi^{1,2,3} · Alejandro Vargas-Uscategui² · Xiaofeng Wu¹ · Peter C. King²

Submitted: 15 June 2023 / in revised form: 22 January 2024 / Accepted: 24 January 2024 / Published online: 9 February 2024
© Crown 2024, corrected publication 2024

Abstract Cold spray additive manufacturing is an emerging solid-state deposition process that enables large-scale components to be manufactured at high-production rates. Control over geometry is important for reducing the development and growth of defects during the 3D build process and improving the final dimensional accuracy and quality of components. To this end, a machine learning approach has recently gained interest in modeling additively manufactured geometry; however, such a data-driven modeling framework lacks the explicit consideration of a depositing surface and domain knowledge in cold spray

additive manufacturing. Therefore, this study presents surface-aware data-driven modeling of an overlapping-track profile using a Gaussian Process Regression model. The proposed Gaussian Process modeling framework explicitly incorporated two relevant geometric features (i.e., surface type and polar length from the nozzle exit to the surface) and a widely adopted Gaussian superposing model as prior domain knowledge in the form of an explicit mean function. It was shown that the proposed model could provide better predictive performance than the Gaussian superposing model alone and the purely data-driven Gaussian Process model, providing consistent overlapping-track profile predictions at all overlapping ratios. By combining accurate prediction of track geometry with toolpath planning, it is anticipated that improved geometric control and product quality can be achieved in cold spray additive manufacturing.

Keywords additive manufacturing · cold spray · gaussian process · machine learning · model · overlap

This article is an invited paper selected from presentations at the 2023 International Thermal Spray Conference, held May 22–25, 2023, in Québec City, Canada, and has been expanded from the original presentation. The issue was organized by Giovanni Bolelli, University of Modena and Reggio Emilia (Lead Editor); Emine Bakan, Forschungszentrum Jülich GmbH; Partha Pratim Bandyopadhyay, Indian Institute of Technology, Karaghpur; Šárka Houdková, University of West Bohemia; Yuji Ichikawa, Tohoku University; Heli Koivuluoto, Tampere University; Yuk-Chiu Lau, General Electric Power (Retired); Hua Li, Ningbo Institute of Materials Technology and Engineering, CAS; Dheepa Srinivasan, Pratt & Whitney and Filofteia-Laura Toma, Fraunhofer Institute for Material and Beam Technology.

✉ Alejandro Vargas-Uscategui
alejandro.vargas@csiro.au

✉ Peter C. King
peter.king@csiro.au

¹ School of Aerospace, Mechanical and Mechatronic Engineering, The University of Sydney, Sydney, NSW 2006, Australia

² CSIRO Manufacturing, Private Bag 10, Clayton, VIC 3169, Australia

³ Department of Engineering, University of Cambridge, Cambridge CB2 1PZ, UK

Introduction

Cold spray is a coating technology in which powder particles are accelerated to 500–1000 m/s to achieve metallurgical bonding without in-flight melting. This solid-state deposition offers unique advantages, such as the absence of melting-induced microstructure changes, a high deposition rate with a narrow nozzle diameter and the possibility of depositing oxygen-sensitive materials without a protective atmosphere (Ref 1–3). Due to these characteristics, cold spray has recently gained interest as additive manufacturing technology and is often referred to as cold spray additive manufacturing (CSAM) (Ref 4–6). CSAM has

considerable potential for large-scale, high-production rate manufacturing and repair on existing surfaces in the aerospace industries (Ref 3, 7).

However, geometric control must be improved for further development of CSAM technology toward commercial applications. As has been pointed out in other high-production rate additive manufacturing (HPRAM) processes, such as wire arc additive manufacturing (WAAM) (Ref 8, 9), poor geometric control poses many practical limitations, including material wastage and geometry-induced property variations (Ref 3, 6). Given the track-by-track nature of HPRAM, a high-accuracy process model based on overlapping-track profiles as the basic geometric unit provides a promising solution to the geometry control issue (Ref 10, 11). Previously, geometric profile modeling in HPRAM was studied using two distinct approaches: mathematical and data-driven modeling, with the former dominating the overlapping-track profile context. In CSAM, a mathematical Gaussian superposing model is usually applied in which a single-track Gaussian function shape is assumed due to the spatial distribution of powder exiting the nozzle and numerically superposed at each trajectory location (Ref 12–15). However, due to the complex processes involved in CSAM (and HPRAM), there is no agreement in the selection of a single mathematical function model (e.g., triangular (Ref 16, 17) and trapezoidal (Ref 18) functions also used in CSAM).

Furthermore, a suitable mathematical function model varies, depending on process parameters and their combination (Ref 19) and coating materials (Ref 10). A data-driven modeling approach has been extensively explored in the recent studies of CSAM geometric modeling due to its superior predictive and continuous learning capabilities for better model performance (Ref 9, 20–22). However, this approach is still poorly explored for overlapping-track profile modeling. Importantly, unlike the single-track modeling case, a data-driven overlapping-track model should incorporate the explicit information of a depositing surface to account for the interaction with the existing deposition (Ref 23–25). This explicit approach is particularly important because deposition onto complex, non-planar surfaces is frequently seen in practice (e.g., repair applications (Ref 26, 27)), and the learning capability of data-driven modeling can handle such complex, and various deposition scenarios as new and unseen circumstances are encountered in manufacturing processes. Another aspect needed for a data-driven overlapping-track model is the greater level of physical insights observed in the mathematical counterparts (e.g., Gaussian distribution of jetted powder in CSAM (Ref 12–14)). As observed in our previous purely data-driven modeling study (Ref 20), incorporating domain knowledge can avoid unusual and inconsistent model prediction and contribute to better predictive performance.

This study uses a surface-aware data-driven modeling approach to predict an overlapping-track profile in CSAM, using a Gaussian Process Regression (GPR) model due to its superior training capability with fewer data (Ref 28, 29) and better predictive accuracy over neural networks in relevant fields (Ref 30). The significance of this study is threefold. Firstly, we integrate two relevant geometric features to incorporate surface awareness in the proposed modeling framework; these features are surface type and the projected polar length to the point of impact that defines depositing surface conditions and influence deposited track profiles. Secondly, we adopt a mathematical Gaussian superposing model as an explicit mean function of the proposed GPR model. This modeling approach introduces an approximated underlying physical representation to leverage as prior domain knowledge that, in turn, achieves the increased level of physical insight as compared to a purely data-driven GPR model. Thirdly, we perform the comparative study among mathematical Gaussian superposing, purely data-driven GPR and proposed GPR approaches in overlapping-track profile modeling and demonstrate that the proposed approach can outperform the mathematical and purely data-driven counterparts. For simplicity, this study focuses on the case of two side-by-side tracks and only applies the predictive model to the 2nd overlapping-track profile.

Materials and Methods

This study selected three experimental process variables to prepare the representative overlapping-track profiles: overlapping ratio (OR), traverse speed and standoff distance. Herein, OR follows the definition by Chen et al. (Ref 31) and represents the ratio of overlap from 0 to 1 between the two adjacent profiles to the width of a single track. Hence, a higher OR indicates a larger overlapping region between the two adjacent profiles. A full factorial design of experiments method was adopted in this study to determine the values of the experimental process variables for the preparation of each experimental condition.

Table 1 lists the level values for each experimental process variable, leading to the fabrication of 36 overlapping-track profiles in the full factorial framework. Additionally, 12 overlapping-track profiles were prepared to ensure the coverage of further interactions between the process variables using a randomly selected combination of the process variables within the defined variable space of Table 1. The default random number generator assisted this random selection in MATLAB version R2018a. The complete list of each experimental condition for a total of 48 overlapping-track profiles is shown in the Supplementary Information. Additionally, we provide the schematic

diagram in Fig. 1 to visualize the major procedures for model development to be presented in this section.

Sample Preparation

A commercial Impact Innovations 5/11 cold spray gun, mounted on and guided by a 6-degree-of-freedom ABB IRB4600 robot, was used to prepare all experimental CSAM samples in this study. The cold spray nozzle was an OUT1 tungsten carbide de Laval type with a 6.2-mm exit diameter. A gas-atomized, commercial purity ASTM grade-2 titanium powder feedstock was used in this study. The powder had a particle size distribution of $D_{10} = 19 \mu\text{m}$, $D_{50} = 34 \mu\text{m}$ and $D_{90} = 45 \mu\text{m}$, measured by laser diffraction. Nitrogen was used as the working gas with preheat temperature of 600 °C at a pressure of 5 MPa.

The powder feedstock was fed into the stagnation zone at a 2.12 kg/h rate. The substrate was a commercial purity ASTM grade-2 titanium strip with $6 \times 30 \times 200 \text{ mm}$ dimensions. The substrate surface was prepared by: processing with a milling machine, grinding with a P120-SiC emery paper and cleaning with ethanol before the experiments. Using ABB RobotStudio version 6.08, it was ensured that the spray path was sufficient to allow the robot trajectory and traverse speed to stabilize before reaching the edge of a substrate.

The geometric measurement of each sample profile was performed at five random locations using a LEXT OLS4000 confocal laser scanning microscope and scanControl 2950-100 laser scanner with a z-axis measurement precision of 12 μm . The in-built filtering methods were applied: flat surface filtering in LEXT OLS4000 and

Table 1 The levels of process variables in the experimental design matrix for preparing overlapping-track profiles in cold spray additive manufacturing

Level	Overlapping ratio	Traverse speed, mm/s	Standoff distance, mm
1	0.3	25	30
2	0.5	100	40
3	0.7	200	50
4	0.9

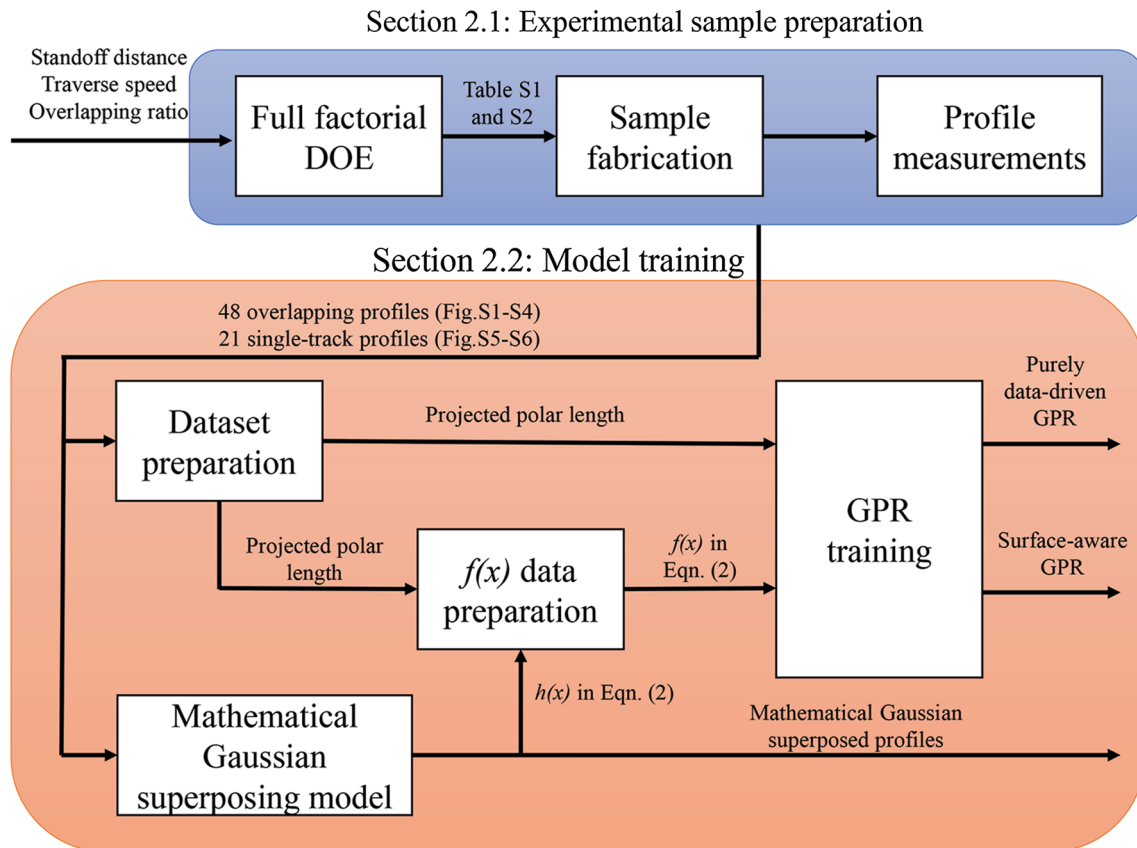


Fig. 1 A schematic diagram showing the overall major procedures and data processing workflow for the proposed overlapping-track profile modeling

average filtering with a filter size of 7 in scanControl Configuration Tool version 6.0, followed by a local regression method using a weighted linear least square and second-order polynomial model in the Curve Fitting Toolbox, MATLAB version R2018a. This method allows for the fitting of track profiles by minimizing the square of residual errors. The five filtered profiles were then averaged to represent each sample profile. In addition to 48 overlapping-track profiles, a single-track profile was prepared following the same method described above at each unique combination of traverse speed and standoff distance in Table S2 in the Supplementary Information (i.e., 21 single-track profiles in total). These single-track profiles represented constituent profiles fabricated during the first tracks and were used to prepare the data that represented the geometric information of a depositing surface for overlapping-track cases as detailed in Section “Modeling strategy and training.”

Modeling Strategy and Training

Figure 2 shows the illustration of a two-track overlapping case in this study. To explicitly incorporate the information about a depositing surface, two relevant geometric features were used: (1) surface type (i.e., whether depositing on the

substrate or first-track profile, classified as -1 or 1 , respectively) and (2) the polar length from the center of the nozzle exit to a projected point on the surface before the second-track deposition, as shown in Fig. 2. In addition, polar angle and traverse speed were selected, giving four input features in total for the proposed GPR model. The polar length change at each polar angle in Fig. 2 was used as the output for the proposed GPR model, as adopted in (Ref 13, 25). The preparation of the input dataset was based on the sampling of geometric points from the single-track profiles at the same process conditions in Fig. S5-S6 in the Supplementary Information. The output dataset was obtained by subtracting these sampled polar lengths from those of the overlapping-track profiles in Fig. S1-S4 in the Supplementary Information. Herein, an assumption was made that the first-track profile could be fabricated with reasonably small geometric deviations using the precisely controlled robotic system. The region of interest for geometric point sampling was selected to ± 5 mm about the tool center point, about 25 % larger than the largest width of the fabricated single-track profile observed during the sample preparation. This selection ensured that the dataset contained relevant and meaningful information while minimizing its size for computational efficiency. Consequently, 151 geometric points were taken from each profile

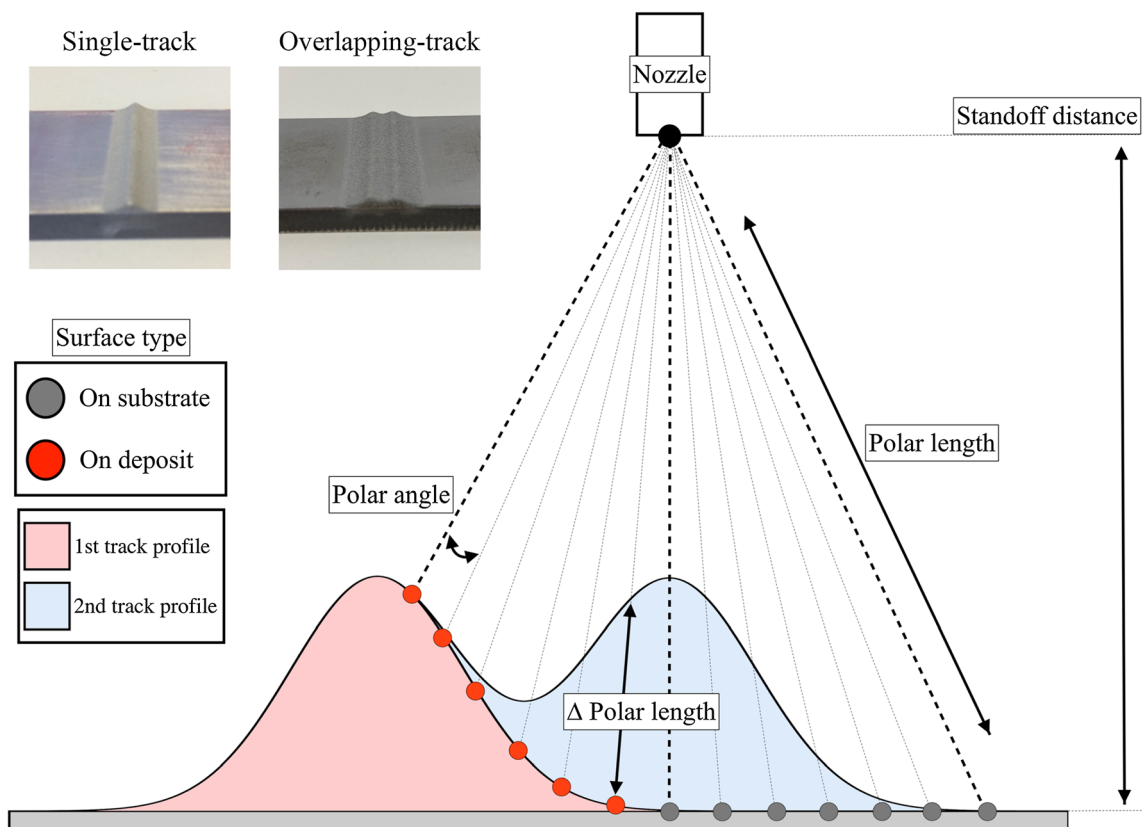


Fig. 2 The proposed overlapping-track modeling schematic (Color figure online)

case, with 1 point at the tool center point and the rest equally distanced on both sides.

GPR is a nonparametric data-driven modeling approach, offering advantages such as the effect of Occam's razor for overfitting avoidance with small datasets (Ref 32). Given the feature vector, x , a GPR model can be fully defined by a mean function, $m(x)$, and covariance function, $k(x, x')$, as in Eq. 1:

$$y(x) = \mathcal{GP}(m(x), k(x, x')) + \epsilon \quad (\text{Eq 1})$$

The proposed GPR model incorporated prior domain knowledge about the expected outcome of a modeled process (i.e., the shape of a track profile) into a deterministic explicit mean function, $h(x)$, in the modified form of Eq. 1 (Ref 33, 34) as expressed in Eq. 2, where $f(x)$ is the data-driven GPR in Eq. 1 trained to learn the deviation between approximate, $h(x)$, and true outputs, $y(x)$.

$$y(x) = h(x) + f(x) + \epsilon = h(x) + \mathcal{GP}(0, k(x, x')) + \epsilon \quad (\text{Eq 2})$$

Using an explicit mean function offers advantages over the direct incorporation of domain knowledge into a mean function, $m(x)$, of Eq. 1, including computational efficiency and predictive performance with limited data (Ref 32, 35). The data-driven GPR model component, $f(x)$, was set with $m(x) = 0$ and Matérn 3/2 covariance function. The prior domain knowledge can serve as an approximated solution that the proposed GPR model provides, avoiding a large and physically inconsistent predictive error from overfitting with limited data observed in our previous studies (Ref 20, 21). A Gaussian superposing model, previously adopted in (Ref 12, 13), was leveraged in this regard with its model coefficients computed by a quadratic regression model. This mathematical model formed expected overlapping-track profiles that assumed particle build-up on the surface to follow Gaussian distribution, following acceleration through a de Laval nozzle with a circular cross-section (Ref 12–15). The details of building this previously proposed Gaussian superposing model are presented in the Supplementary Information.

All input and output features were normalized to $[-1, 1]$ to generalize different input scales. This data-driven $f(x)$ component was trained using Statistics and Machine Learning Toolbox in MATLAB version R2018a. The standard marginal log-likelihood maximization was used as a training method with the default subset of regressors approximation to avoid the computational burden of kernel matrix inversion. The data-driven $f(x)$ component was retrained ten times to avoid the convergence to local optima due to the initial values of hyperparameters. This study adopted k -fold cross-validation with $k = 5$, as previously used in the relevant manufacturing field (Ref 36), to evaluate the generalized predictive performance of the

proposed GPR modeling approach using a mean squared error (MSE). For predictive performance comparison, this study also developed a purely data-driven GPR model in Eq. 1, following the above procedures for the proposed GPR modeling approach.

Results and Discussion

The quality of experimental overlapping-track profiles was validated against the previous CSAM studies through the effect of the three process variables on geometric deposit formation in Table 1. This validation was done to confirm that consistent effects of the process variables were observed and, therefore, ensure that the quality of the experimental overlapping-track profiles was sufficient to generate relevant and meaningful datasets containing the true representation of the CSAM process for the development of data-driven models in this study that could be implemented in practical applications.

Figure 3 shows the constituent single- and overlapping-track profile of the selected profiles, as an illustration, by varying: (a) traverse speed at 30-mm standoff distance, (b) standoff distance at 25-mm/s traverse speed and (c) OR at 25-mm/s traverse speed and 30-mm standoff distance. Note that all experimental constituent single- and overlapping-track profiles are shown in Fig. S1–S6 in the Supplementary Information.

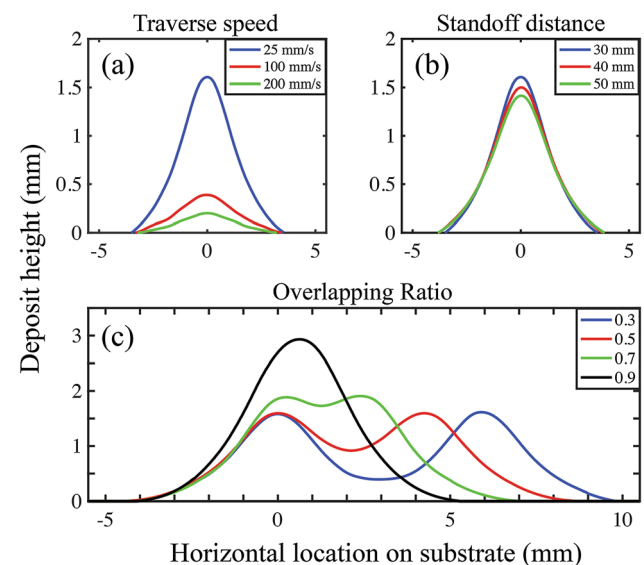


Fig. 3 The quality validation of experimental overlapping-track profiles through the effect of varying: (a) traverse speed (25 mm/s, 100 mm/s and 200 mm/s), (b) standoff distance (30 mm, 40 mm and 50 mm) and (c) overlapping ratio (0.3, 0.5, 0.7 and 0.9) (Color figure online)

Figure 3a shows that the effect of traverse speed was negatively correlated to both the width and height of the constituent single-track profiles, as previously observed in (Ref 6, 12). In contrast, standoff distance was positively and negatively correlated with the width and height, respectively, consistent with another CSAM study (Ref 37). In Fig. 3b, standoff distance was found to have a lesser influence on deposit geometry formation due to the distance values chosen in this study lying within an optimum range as far as deposition efficiency is concerned, as shown in (Ref 38). In Fig. 3c, an observed trend at low ORs was that the shape of a constituent first-track profile was rather retained, with the peak height of the resulting overlapping-track profile being similar. The same trend was identified up to OR = 0.5 in the recent CSAM overlapping modeling study (Ref 18). Beyond this OR, the two adjacent track profiles tended to combine and even form a higher single-peak overlapping profile at OR = 0.9. Figure 3c shows that the height of the resulting overlapping profile at OR = 0.7 and 0.9 was higher than that of a constituent first-track profile, and the peak height shifted toward the overlapping-track profile side. These trends were seen in the previous cold spray studies (Ref 12, 18). The results in Fig. 3 confirm the quality of the fabricated experimental CSAM profiles and therefore the resulting dataset for data-driven modeling in this study.

The data-driven GPR component, $f(x)$, mapping the deviation between the approximate, $h(x)$, and true polar length change, $y(x)$, was built and iteratively evaluated within the cross-validation framework, resulting in the predictive performance on independent testing datasets with an MSE of 0.003573. The individual prediction results of $f(x)$ are plotted in Fig. 4a, showing the linear fit with $R^2 = 0.9299$ to the normalized target outputs.

The proposed GPR model, $y(x)$, in Eq. 2 incorporating the explicit mean function, $h(x)$, and data-driven GPR component, $f(x)$, above, was shown to achieve the normalized predictive performance with an MSE of 0.0002183. The resulting mean and maximum absolute percent error, MAPE and MXAPE, respectively, were found to be 0.5748% and 6.910%, with each prediction result being plotted in Fig. 4b and showing $R^2 = 0.9988$. These results were sufficient in comparison with other data-driven modeling studies in HPRAM (e.g., MXAPE of 4.29% in WAAM (Ref 39) and $R^2 = 0.99575$ in CSAM (Ref 25)).

Furthermore, the proposed GPR models were evaluated and compared against other modeling approaches, including the mathematical Gaussian superposing model and purely data-driven GPR models. Herein, the Gaussian superposing model was based on the optimal coefficients found through the curve-fitting method and listed in Table S3 in the Supplementary Information, but not on the

coefficients computed by the quadratic regression model for forming the explicit mean function, $h(x)$, in the proposed GPR models. The resulting model was referred to as the curve-fitted Gaussian superposing model and prepared to compare the proposed GPR modeling approach against the best possible predictive performance achievable within the previously proposed mathematical framework (Ref 12, 13).

The prediction results of each modeling approach are summarized in Table 2. Compared with the curve-fitted Gaussian superposing model, both the purely data-driven GPR and proposed GPR models showed better predictive performance; the former achieved 33.8% and 19.1% improvements, while the latter outperformed with 73.7% and 64.1% improvements in MAPE and MXAPE, respectively. This observation supports the effectiveness of explicitly incorporating depositing surface information (or surface awareness) into the modeling framework in complex HPRAM processes. Among the data-driven modeling approaches, the proposed GPR model outperformed overall with 60.3% and 55.7% improvements in MAPE and MXAPE, respectively. Notably, the upper 25% quartile was more than twice narrower than the purely data-driven GPR. This result could be due to incorporating physical insights as the explicit mean function in the proposed GPR model, avoiding large physically inconsistent predictions even in the data-scarce regime of CSAM processes (e.g., around peak regions of track profiles as observed in our previous study [20, 21]).

Figure 5 shows the four selected overlapping-track profiles in CSAM as an illustration of each OR stated in Table 1: (a) OR = 0.3, (b) OR = 0.5, (c) OR = 0.7 and (d) OR = 0.9. Note that all the prediction results by each model are shown in Fig. S1-S4 in the Supplementary Information. The proposed GPR models showed reasonably accurate profile predictions at all ORs in Fig. 5 and particularly performed better than the purely data-driven GPR models at high ORs. This observation supported the results in Table 2, showing the mitigated effect of the data scarcity issue around high-profile regions, particularly at high ORs, observed in our previous study (Ref 20, 21). Compared to the curve-fitted Gaussian superposing model, the proposed GPR models showed better predictive performance at all ORs in Fig. 5, especially in the overlapping regions. This observation may be attributed to the proposed data-driven modeling approach capturing complex physical phenomena related to deposition in these regions in CSAM. One example of that complexity is a sharpening of the track profile observed when it grows in height—a shape described as “triangle-like.” This shape results from reduced deposition efficiency onto sloped surfaces and lower particle impact velocity at the peripheries due to the interaction between the gas jet and the deposit surface (Ref 16).

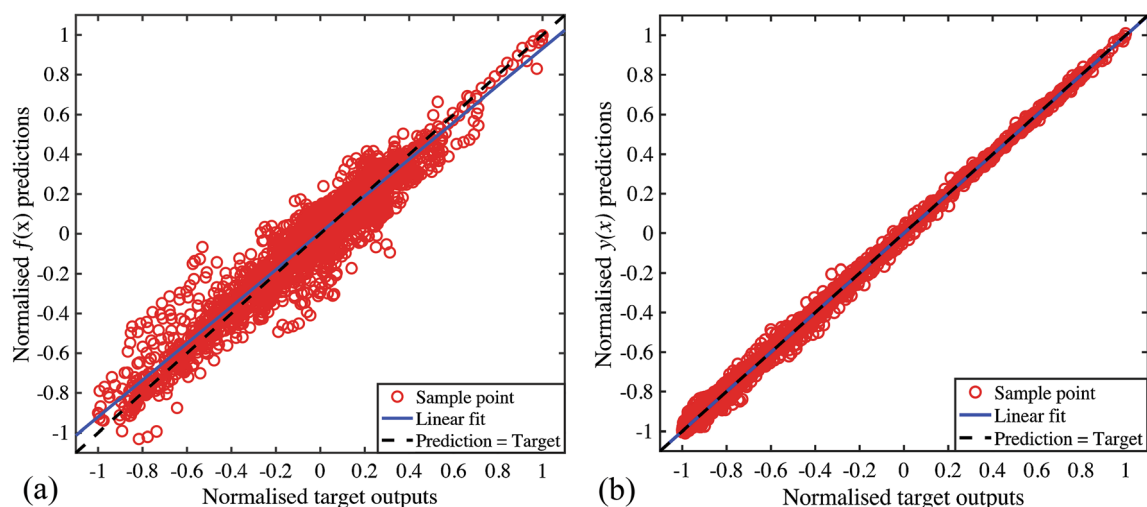


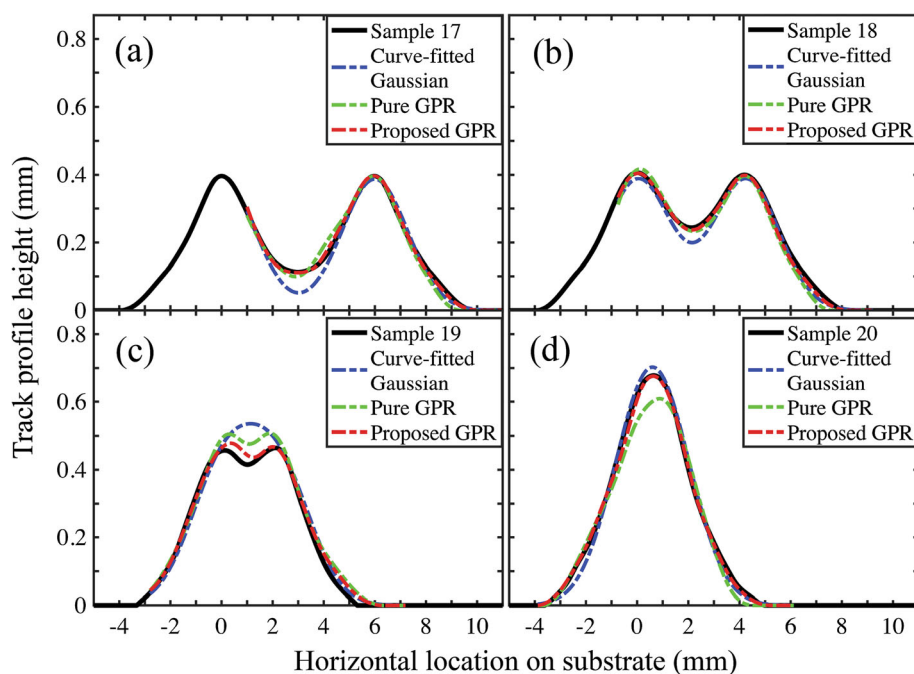
Fig. 4 The results of normalized predictions vs. target outputs: (a) the data-driven GPR component, $\langle i \rangle f(x) \langle /i \rangle$, computing the deviations from actual polar length changes with a mean squared error of 0.003573 and (b) the proposed GPR model, $\langle i \rangle y(x) \langle /i \rangle$,

incorporating $\langle i \rangle f(x) \langle /i \rangle$ and explicit mean function, $\langle i \rangle h(x) \langle /i \rangle$, with a mean squared error of 0.0002183 (Color figure online)

Table 2 Summary of prediction results in absolute errors for the second-order overlapping-track profiles. The results were obtained from the mathematical Gaussian superposing model, purely data-driven GPR models and the proposed GPR models. R^2 values are also listed

Absolute error, %	Gaussian superposing model	Purely data-driven GPR	Proposed GPR
Mean	2.189	1.449	0.575
Minimum	1.3950×10^{-4}	0.5395×10^{-4}	0.2255×10^{-4}
Lower Q	0.3828	0.2687	0.0609
Median	1.140	0.801	0.233
Upper Q	2.548	1.846	0.682
Maximum	19.26	15.59	6.91
R^2	0.9813	0.9909	0.9988

Fig. 5 The experimental overlapping-track profiles of four selected samples as illustrative cases (black) plotted with the corresponding prediction results of the curve-fitted Gaussian superposing model (blue), purely data-driven GPR model (green) and the proposed GPR model (red): (a) Sample 17 (OR = 0.3), (b) Sample 18 (OR = 0.5), (c) Sample 19 (OR = 0.7) and (d) Sample 20 (OR = 0.9), all at the traverse speed of 100 mm/s and the standoff distance of 30 mm. The sample IDs correspond to those listed in Table S1 in the Supplementary Information (Color figure online)



This result was seen in previous CSAM modeling studies, demonstrating that a mathematical superposing model would not be adequate in every case (Ref 12, 20, 37, 40).

The curve-fitted Gaussian superposing model computed a lower overlapping-track profile at low ORs in Fig. 5a and b. These results demonstrated that a simple mathematical function framework, not explicitly incorporating relevant depositing surface information, failed to account for the changes in deposition efficiency around the overlapping regions. For example, the lower effective standoff distance and higher relative spray angle at the impact points increased deposition efficiency at the overlapping regions (Ref 6, 27). Therefore, the resulting experimental overlapping-track profiles were higher than the Gaussian superposing model predicted.

In contrast, the Gaussian superposing model showed a higher overlapping-track profile at high ORs, consistent with the previous cold spray and CSAM studies (Ref 12, 13, 37). This observation may be related to the lack of a handling capability for deposition efficiency changes in CSAM. One potentially influential factor here was surface roughness. It has been reported that deposition efficiency is directly proportional to roughness (Ref 41). This effect may combine with lower effective spray angles at high ORs, cancelling the increased deposition efficiency due to the rougher depositing surface and the shorter effective standoff distance, leading to a smaller deviation at OR = 0.9 than OR = 0.7.

Conclusions

This study presented a data-driven modeling approach that explicitly incorporated surface awareness and prior domain knowledge to predict an overlapping-track profile in CSAM. A comparative study was also performed between the Gaussian superposing, purely data-driven and proposed GPR models; the proposed GPR modeling approach achieved more than 50% improvement than the counterparts in both MAPE and MXAPE with no significantly inconsistent predictions. These results suggest that integrating the geometrically relevant features and prior domain knowledge was effective. Although this study harnessed a widely adopted mathematical function model, the proposed approach can be applied to any existing models (e.g., purely data-driven ANN from our previous CSAM study (Ref 20)) and extended to other HPRAM processes with an appropriate alternative model, e.g., the mathematical parabolic function model used in WAAM (Ref 42). Harnessing such prior domain knowledge based on the underlying physical phenomenon would help maintain the predictive accuracy in the scenarios where the

available data are scarce (e.g., outside the parameter range covered in the original dataset).

Although this study focused on a set gas temperature and pressure, powder size distribution and morphology, the proposed modeling approach applies to other cold spray settings, provided a suitable dataset is available. To this end, the study will be extended in future work with the development of an appropriate online measurement system such as (Ref 43) to allow for efficient in situ data collection of the relevant geometric features under various parameter combinations and for generalizing to 3D multi-track and multi-layer cases. The proposed modeling approach is expected to handle more complex deposition, repairing and manufacturing scenarios which fully realize its strength with explicit surface awareness. For example, incorporating polar lengths as inputs allows direct application to complex surface topologies and off-normal spray angles, and it is compatible with ray-casting methods for predicting line-of-sight deposition. Further, the surface type classification may account for deposition onto different and multiple coating/substrate material combinations. The resulting 3D model will then be combined with our recent work on toolpath planning strategy to enable an industrially acceptable level of geometric control through on-the-fly parameter adjustment in real time to develop and implement CSAM technology (Ref 44).

Supplementary Information The online version contains supplementary material available at <https://doi.org/10.1007/s11666-024-01733-3>.

Acknowledgments This work was supported by CSIRO's Active Integrated Matter Future Science Platform (AIM-FSP). Daiki Ikeuchi received Research Training Program (International) Scholarship from the Department of Education, Skills and Employment, Australia. The authors thank CSIRO Characterization for access to LEXT OLS4000 conformal laser scanning microscope.

Funding Open access funding provided by CSIRO Library Services.

Open Access This article is licensed under a Creative Commons Attribution 4.0 International License, which permits use, sharing, adaptation, distribution and reproduction in any medium or format, as long as you give appropriate credit to the original author(s) and the source, provide a link to the Creative Commons licence, and indicate if changes were made. The images or other third party material in this article are included in the article's Creative Commons licence, unless indicated otherwise in a credit line to the material. If material is not included in the article's Creative Commons licence and your intended use is not permitted by statutory regulation or exceeds the permitted use, you will need to obtain permission directly from the copyright holder. To view a copy of this licence, visit <http://creativecommons.org/licenses/by/4.0/>.

References

- F. Gärtner, T. Stoltenhoff, T. Schmidt, and H. Kreye, The Cold Spray Process and Its Potential for Industrial Applications, *J. Therm. Spray Technol.*, 2006, **15**(2), p 223-232.
- X.-T. Luo, C.-X. Li, F.-L. Shang, G.-J. Yang, Y.-Y. Wang, and C.-J. Li, High Velocity Impact Induced Microstructure Evolution during Deposition of Cold Spray Coatings: A Review, *Surf. Coat. Technol.*, 2014, **254**, p 11-20.
- G. Prashar and H. Vasudev, A Comprehensive Review on Sustainable Cold Spray Additive Manufacturing: State of the Art, Challenges and Future Challenges, *J. Clean. Prod.*, 2021, **310**, p 127606.
- S. Pathak and G. Saha, Development of Sustainable Cold Spray Coatings and 3D Additive Manufacturing Components for Repair/Manufacturing Applications: A Critical Review, *Coatings*, 2017, **7**(122), p 1-27.
- W. Li, K. Yang, S. Yin, X. Yang, Y. Xu, and R. Lupoi, Solid-State Additive Manufacturing and Repairing by Cold Spraying: A Review, *J. Mater. Sci. Technol.*, 2018, **34**(3), p 440-457.
- S. Yin, P. Cavaliere, B. Aldwell, R. Jenkins, H. Liao, W. Li, and R. Lupoi, Cold Spray Additive Manufacturing and Repair: Fundamentals and Applications, *Addit. Manuf.*, 2018, **21**, p 628-650.
- K.S. Aggour, V.K. Gupta, D. Ruscitto, L. Ajdelsztajn, X. Bian, K.H. Brosnan, N. Chennimalai Kumar, V. Dheeradhada, T. Hanlon, N. Iyer, J. Karandikar, P. Li, A. Moitra, J. Reimann, D.M. Robinson, A. Santamaria-Pang, C. Shen, M.A. Soare, C. Sun, A. Suzuki, R. Venkataramana, and J. Vinciguerra, Artificial Intelligence/Machine Learning in Manufacturing and Inspection: A GE Perspective, *MRS Bull.*, 2019, **44**(7), p 545-558.
- Y. Li, X. Li, G. Zhang, I. Horváth, and Q. Han, Interlayer Closed-Loop Control of Forming Geometries for Wire and Arc Additive Manufacturing Based on Fuzzy-Logic Inference, *J. Manuf. Process.*, 2020, **63**, p 35-47.
- C. Xia, Z. Pan, J. Polden, H. Li, Y. Xu, and S. Chen, Modelling and Prediction of Surface Roughness in Wire Arc Additive Manufacturing Using Machine Learning, *J. Intell. Manuf.*, 2021, **33**, p 1467-1482.
- L.E. dos Santos Paes, H.S. Ferreira, M. Pereira, F.A. Xavier, W.L. Weingaertner, and L.O. Vilarinho, Modeling Layer Geometry in Directed Energy Deposition with Laser for Additive Manufacturing, *Surf. Coat. Technol.*, 2021, **409**, p 126897.
- O. Nenadl, W. Kuipers, N. Koelewijn, V. Ocelík, and J.T.M. De Hosson, A Versatile Model for the Prediction of Complex Geometry in 3D Direct Laser Deposition, *Surf. Coat. Technol.*, 2016, **307**, p 292-300.
- C. Chen, Y. Xie, C. Verdy, H. Liao, and S. Deng, Modelling of Coating Thickness Distribution and Its Application in Offline Programming Software, *Surf. Coat. Technol.*, 2017, **318**, p 315-325.
- H. Wu, X. Xie, M. Liu, C. Chen, H. Liao, Y. Zhang, and S. Deng, A New Approach to Simulate Coating Thickness in Cold Spray, *Surf. Coat. Technol.*, 2020, **382**, p 125151.
- H. Wu, X. Xie, M. Liu, C. Verdy, Y. Zhang, H. Liao, and S. Deng, Stable Layer-Building Strategy to Enhance Cold-Spray-Based Additive Manufacturing, *Addit. Manuf.*, 2020, **35**, p 101356.
- I.M. Nault, G.D. Ferguson, and A.T. Nardi, Multi-Axis Tool Path Optimization and Deposition Modeling for Cold Spray Additive Manufacturing, *Addit. Manuf.*, 2021, **38**, p 101779.
- D. Kotoban, S. Grigoriev, A. Okunkova, and A. Sova, Influence of a Shape of Single Track on Deposition Efficiency of 316L Stainless Steel Powder in Cold Spray, *Surf. Coat. Technol.*, 2017, **309**, p 951-958.
- S.V. Klinkov, V.F. Kosarev, and V.S. Shikalov, Influence of Nozzle Velocity and Powder Feed Rate on the Coating Mass and Deposition Efficiency in Cold Spraying, *Surf. Coat. Technol.*, 2019, **367**, p 231-243.
- W. Zhu, X. Zhang, M. Zhang, X. Tian, and D. Li, Integral Numerical Modeling of the Deposition Profile of a Cold Spraying Process as an Additive Manufacturing Technology, *Prog. Addit. Manuf.*, 2019, **4**(4), p 357-370.
- J. Xiong, G. Zhang, H. Gao, and L. Wu, Modeling of Bead Section Profile and Overlapping Beads with Experimental Validation for Robotic GMAW-Based Rapid Manufacturing, *Robot. Comput. Integr. Manuf.*, 2013, **29**(2), p 417-423.
- D. Ikeuchi, A. Vargas-Uscategui, X. Wu, and P.C. King, Neural Network Modelling of Track Profile in Cold Spray Additive Manufacturing, *Materials*, 2019, **12**(17), p 2827.
- D. Ikeuchi, A. Vargas-Uscategui, X. Wu, and P. King, Data-Efficient Neural Network for Track Profile Modelling in Cold Spray Additive Manufacturing, *Appl. Sci.*, 2021, **11**(4), p 1654.
- K. Malamousi, K. Delibasis, B. Allcock, and S. Kamnis, Digital Transformation of Thermal and Cold Spray Processes with Emphasis on Machine Learning, *Surf. Coat. Technol.*, 2022, **433**, p 128138.
- T. Chen, W. Wu, W. Li, and D. Liu, Laser Cladding of Nanoparticle TiC Ceramic Powder: Effects of Process Parameters on the Quality Characteristics of the Coatings and Its Prediction Model, *Opt. Laser Technol.*, 2019, **116**, p 345-355.
- K. Aggarwal, R.J. Urbanic, and S.M. Saqib, Development of Predictive Models for Effective Process Parameter Selection for Single and Overlapping Laser Clad Bead Geometry, *Rapid Prototyp. J.*, 2018, **24**(1), p 214-228.
- M. Liu, H. Wu, Z. Yu, H. Liao, and S. Deng, Description and Prediction of Multi-Layer Profile in Cold Spray Using Artificial Neural Networks, *J. Therm. Spray Technol.*, 2021, **30**(6), p 1453-1463.
- M. Tzinava, K. Delibasis, B. Allcock, and S. Kamnis, A General-Purpose Spray Coating Deposition Software Simulator, *Surf. Coat. Technol.*, 2020, **399**, p 126148.
- M. Jeandin, F. Delloro, and M. Bunel, Advanced Modeling and Simulation Tools to Address Build-Up Issues in Additive Manufacturing by Cold Spray, *Cold Spray in the Realm of Additive Manufacturing*. S. Pathak, G.C. Saha Ed., Springer, Cham, 2020, p 129-175.
- S. Wang, L. Zhu, J.Y.H. Fuh, H. Zhang, and W. Yan, Multi-Physics Modeling and Gaussian Process Regression Analysis of Cladding Track Geometry for Direct Energy Deposition, *Opt. Lasers Eng.*, 2020, **127**, p 105950.
- S. Mondal, D. Gwynn, A. Ray, and A. Basak, Investigation of Melt Pool Geometry Control in Additive Manufacturing Using Hybrid Modeling, *Metals*, 2020, **10**(5), p 683.
- Y. Zhang and X. Xu, Predicting the Material Removal Rate during Electrical Discharge Diamond Grinding Using the Gaussian Process Regression: A Comparison with the Artificial Neural Network and Response Surface Methodology, *Int. J. Adv. Manuf. Technol.*, 2021, **113**(5-6), p 1527-1533.
- C. Chen, G. Lian, J. Jiang, and Q. Wang, Simplification and Experimental Investigation of Geometrical Surface Smoothness Model for Multi-Track Laser Cladding Processes, *J. Manuf. Process.*, 2018, **36**, p 621-628.
- C.E. Rasmussen and C.K.I. Williams, *Gaussian Processes for Machine Learning*, The MIT Press, Cambridge, Massachusetts, 2006.
- F. Massa Gray and M. Schmidt, A Hybrid Approach to Thermal Building Modelling Using a Combination of Gaussian Processes and Grey-Box Models, *Energy Build.*, 2018, **165**, p 56-63.

34. Ren, Y., Wang, Q., and Michaleris, P., 2019, “Machine-Learning Based Thermal-Geometric Predictive Modeling of Laser Powder Bed Fusion Additive Manufacturing,” *Proceedings of the ASME 2019 Dynamic Systems and Control Conference*, ASME, pp. 1–10.
35. E. Schulz, M. Speekenbrink, and A. Krause, A Tutorial on Gaussian Process Regression: Modelling, Exploring, and Exploiting Functions, *J. Math. Psychol.*, 2018, **85**, p 1–16.
36. G. Tapia, S. Khairallah, M. Matthews, W.E. King, and A. Elwany, Gaussian Process-Based Surrogate Modeling Framework for Process Planning in Laser Powder-Bed Fusion Additive Manufacturing of 316L Stainless Steel, *Int. J. Adv. Manuf. Technol.*, 2018, **94**(9–12), p 3591–3603.
37. Z. Cai, S. Deng, H. Liao, C. Zeng, and G. Montavon, The Effect of Spray Distance and Scanning Step on the Coating Thickness Uniformity in Cold Spray Process, *J. Therm. Spray Technol.*, 2014, **23**(3), p 354–362.
38. J. Pattison, S. Celotto, A. Khan, and W. O’Neill, Standoff Distance and Bow Shock Phenomena in the Cold Spray Process, *Surf. Coat. Technol.*, 2008, **202**(8), p 1443–1454.
39. Deng, J., Xu, Y., Zuo, Z., Hou, Z., and Chen, S., 2019, “Bead Geometry Prediction for Multi-Layer and Multi-Bead Wire and Arc Additive Manufacturing Based on XGBoost,” *Transactions on Intelligent Welding Manufacturing*, S. Chen, Y. Zhang, and Z. Feng, eds., Springer Singapore, Singapore, pp. 125–135.
40. F. Venturi, N. Gilfillan, and T. Hussain, A Convolution-Based Approach to Cold Spray Additive Manufacturing, *Addit. Manuf. Lett.*, 2021, **1**, p 100014.
41. R. Singh, K.-H. Rauwald, E. Wessel, G. Mauer, S. Schrufer, A. Barth, S. Wilson, and R. Vassen, Effects of Substrate Roughness and Spray-Angle on Deposition Behavior of Cold-Sprayed Inconel 718, *Surf. Coat. Technol.*, 2017, **319**, p 249–259.
42. F. Caiazzo and V. Alfieri, Simulation of Laser-Assisted Directed Energy Deposition of Aluminum Powder: Prediction of Geometry and Temperature Evolution, *Materials*, 2019, **12**(13), p 2100.
43. H. Wu, S. Liu, Y. Zhang, H. Liao, R.-N. Raelison, and S. Deng, New Process Implementation to Enhance Cold Spray-Based Additive Manufacturing, *J. Therm. Spray Technol.*, 2021, **30**, p 1284–1293.
44. A. Vargas-Uscategui, P.C. King, S. Yang, C. Chu, and J. Li, Toolpath Planning for Cold Spray Additively Manufactured Titanium Walls and Corners: Effect on Geometry and Porosity, *J. Mater. Process. Technol.*, 2021, **298**, p 117272.

Publisher’s Note Springer Nature remains neutral with regard to jurisdictional claims in published maps and institutional affiliations.